2025 IEEE/SICE International Symposium on System Integration (SII)
January 21-24, 2025, Munich, Germany

Basic Study for Drive Mechanism with Synthetic Fiber Rope: Development of a Tensioning Mechanism using a One-way Clutch and Hose Clamp

Hana Ito[1], Kurumi Osawa[1], Akifumi Okubo[1], and Gen Endo[1]

***Abstract*— The utilization of synthetic fiber ropes in robot driving systems facilitates designs that are more lightweight and compact compared to their stainless steel counterparts. However, rope elongation during operation results in tension loss, necessitating a rope tensioning system to wind the rope and maintain adequate tension. We have previously proposed a tensioning mechanism wherein two shafts are coaxially connected via a one-way clutch, allowing rotation only in the direction of rope tension for fine-tuning the winding length. Nevertheless, this method subjects the one-way clutch to the full torque generated by rope tension. Consequently, if the torque exceeds the allowable limit during locomotion, the one-way clutch may sustain damage due to impact torque. To address this limitation, this study proposes a novel mechanism that integrates a one-way clutch and a hose clamp to enhance the load-bearing capacity of the tensioning mechanism. Furthermore, experimental result suggests that the allowable torque of the tensioner can be significantly increased by introducing a wire mesh between the hose clamp and the shaft, thereby augmenting the friction coefficient of the fastening component.**

I. Introduction

In recent years, there has been significant development in robots driven by synthetic fiber ropes. Compared to stainless steel wires, those ropes are lightweight, high-strength, and allow for smaller bending radii, enabling more compact designs. However, a notable issue is the decrease in joint stiffness due to rope elongation over time. Consequently, a tensioning mechanism is necessary to maintain rope tension through periodic winding. While idlers generally used to apply tension to the wires including synthetic fiber ropes [1] [2], this approach often leads to an increase in size due to the required space.

Previous research has developed lightweight, high-capacity ring tensioners [3], but these have limitations in handling high loads and maximum winding length. Another approach involves winding the rope around a pulley and securing it to the robot body with a hexagonal pin [4]. While this method has been applied to robotic arms, manually applying significant tension to the rope by rotating the pulley is often challenging. Additionally, the hexagonal pin allows for adjustments only in 60-degree increments, making it difficult to maintain adequate tension during fixation. A ratchet clutch-based tensioner has also been developed, allowing unidirectional rotation for rope tension adjustment [5]. This method permits finer adjustments compared to the hexagonal pin approach, but the rotation angle is still constrained by the number of ratchet teeth. In compact designs, the limited number of teeth restricts fine tension adjustments. Conversely, the tensioner used in the quadruped robot TITAN-XIII [6] [7], developed by our research group, employs a roller-type one-way clutch. This design allows for axis rotation only in the tension-increasing direction and enables fixation at any position, facilitating precise tension adjustments. However, as the one-way clutch alone bears the full torque from rope tension, it risks damage if impulse forces during locomotion cause the torque to exceed its allowable limit.

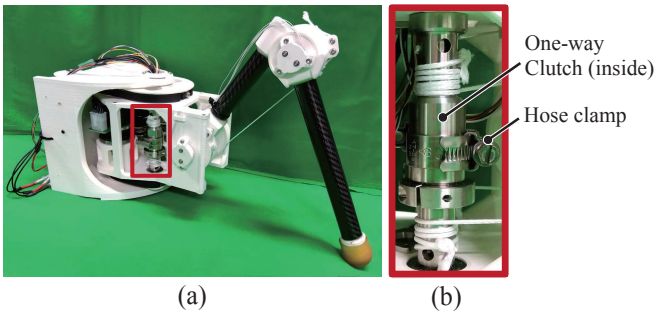

Fig. 1. Prototype of the proposed tensioning mechanism. (a) Applied to TITAN-E1 monopod testing machine. (b) Enlarged view of the tensioner.

To address these issues, we propose a tensioning mechanism that combines a one-way clutch with a hose clamp, as illustrated in Fig. 1. This design aims to support rope tension beyond the capacity of the one-way clutch alone. The objective of this study is to measure the allowable torque of the proposed tensioning mechanism and evaluate its applicability to walking robots.

Chapter 2 elucidates the limitations of conventional tensioning mechanisms and introduce the novel mechanism proposed in this study. Chapter 3 describes the experimental methodology employed to assess the efficacy of the proposed mechanism, focusing on the allowable torque, and present the result. Chapter 4 offers a comprehensive discussion of the findings. Finally, Chapter 5 provides a concise conclusion and suggesting potential avenues for future investigation.

II. Rope Tentioning Mechanism

A. Wire drive mechanism

This section describes the wire drive mechanism employed in TITAN-XIII [6] [7] and TITAN-E1 [8], quadruped robots with reptile-like locomotion featuring 3 degrees of freedom

[1]Hana Ito, Kurumi Osawa, Akifumi Okubo and Gen Endo are with the Department of Mechanical Engineering, Institute of Science Tokyo, 2-12-1 Ookayama, Meguro-ku, Tokyo 152-8550, Japan. ito.h.7e44@m.isct.ac.jp

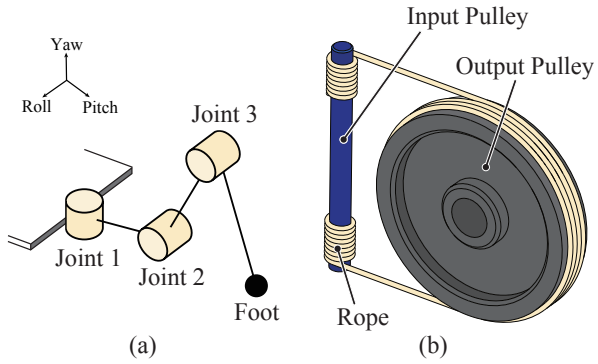

Fig. 2. The leg mechanism of TITAN-XIII and TITAN-E1. (a) Structure of a leg. (b) Wire drive mechanism for Joint 2 and Joint 3.

(DoF) per leg, as illustrated in Fig. 2 (a). Notably, Joint2 and Joint3 are wire-driven by synthetic fiber ropes. Fig. 2 (b) provides an overview of the system.

The wire drive mechanism strategically positions the motor at the base of the leg, significantly reducing the mass of the leg extremities and consequently facilitating more rapid and energy-efficient locomotion. Moreover, when utilized as the final stage of the reduction mechanism, this wire-driven system can distribute load across the entire pulley surface and transmit power without backlash. The synthetic fiber rope employed as the wire offers advantages over stainless steel wire, being both lighter and capable of accommodating a smaller minimum bending radius. This characteristic enables the use of pulleys with reduced diameters compared to conventional wire drive mechanisms. Consequently, as depicted in Fig. 2 (b), the input pulley diameter can be minimized, and the entire mechanism can be designed more compactly by orienting the input pulley perpendicular to the output pulley. This configuration results in a wire-driven mechanism that is both compact and possesses a high reduction ratio: 8.5:1 for TITAN-XIII. The input pulley, around which the rope is wound, is driven by the motor via a timing belt. To compensate for wire elongation, which is an inherent characteristic of synthetic fiber ropes, the wire drive mechanism necessitates a tensioning system. In this design, the input pulley ingeniously serves this dual function of power transmission and tension maintenance.

B. Conventional tensioning mechanism

The conventional tensioning mechanism employed in the aforementioned wire drive system is illustrated in Fig. 3. This mechanism comprises two shafts, denoted as (i) and (ii), around which the rope is wound via output pulleys. A one-way clutch is press-fitted within shaft (i), facilitating a coaxial connection between shafts (i) and (ii). This configuration ensures that relative rotation between the two shafts occurs exclusively in the direction that increases rope tension. The application of an external torque enables the winding of arbitrary rope lengths, thus permitting continuous and precise adjustment of rope tension.

However, a significant limitation of this mechanism is that the only one-way clutch bears the full torque generated

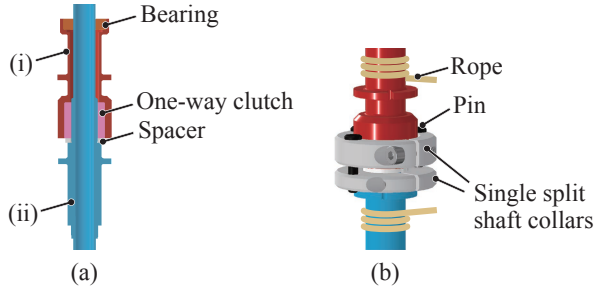

Fig. 3. Conventional rope tensioning mechanism. (a) Cross-sectional view. (b) A modified version of (a) that uses single split shaft collars and pins to fasten shafts (i) and (iii) together to distribute torque.

by the rope tension. In the case of TITAN-E1, a one-way clutch (HF1216, SCHAEFFLER) with an allowable torque of 12.2 Nm was used. However, it has been observed that after prolonged walking periods, the one-way clutch would sustain damage. This is likely due to the impact force at the moment of landing, causing the torque on the tensioner to exceed the allowable limit. Consequently, tensioning mechanisms used in walking robots require even greater allowable torque. While enlarging the one-way clutch diameter could enhance the allowable torque, this would lead to excessive dimensions and mass. Therefore, the one-way clutch remains unchanged.

To address this issue, a modified version of the mechanism was developed, as shown in Fig. 3 (b). This design aims to distribute the torque that was previously borne solely by the one-way clutch by connecting shafts (i) and (ii). Single split shaft collars are tightened on the outer and inner shafts, and pins are inserted to fix the relative positions of those. The rope tensioning process involves removing the shaft collars, tightening the rope, and then reattaching the shaft collars, allowing for fixation at any winding amount.

However, this modified design requires tightening two shaft collars for each tensioner. The overall dimensions of the shaft collar section are 38 mm in outer diameter, 19 mm in height, and 39.7 g in total weight, resulting in a larger and heavier mechanism. Additionally, due to the tolerance relationship between the pins and holes, it is challenging to ensure that all three pins bear the load equally. These limitations necessitate the development of an improved tensioning mechanism that can withstand higher torques while maintaining a lightweight and compact design.

C. Proposal of new tensioning mechanism

The proposed tensioning mechanism is illustrated in Fig. 4. Its fundamental structure is similar to conventional mechanisms. A one-way clutch is press-fitted into shaft (i), which is coaxially connected to shaft (ii) via this clutch. Consequently, these two shafts can only rotate in the direction that increases rope tension. Shaft (iii) is connected to shaft (ii) with a key fixing in the rotational direction and a shaft collar in the axial direction. The operational procedure is as follows: First, both ends of the rope are threaded through and secured in holes drilled in shafts (i) and (iii), then wound around the shafts. Each shaft has four equidistant holes; those not used for rope fixation can accommodate a round bar, which is used to rotate

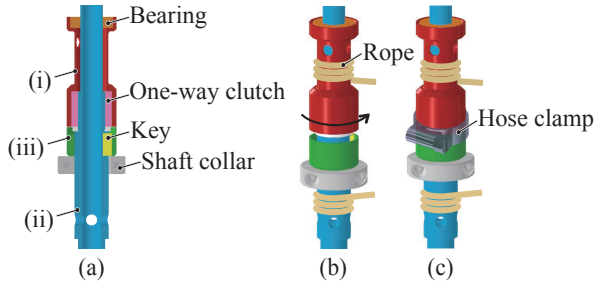

Fig. 4. Proposed rope tensioning mechanism. (a) Cross-sectional view. (b) During rope winding. (c) After winding the rope, tighten the hose clamps to fix the relative positions of shafts (i) and (iii).

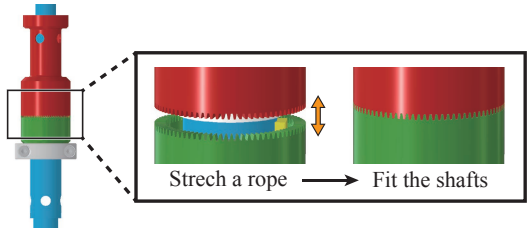

Fig. 5. Another tensioning mechanism examined.

the shafts relative to each other, thereby increasing tension. After tensioning the rope, shafts (i) and (iii) are secured with a hose clamp. This configuration allows the torque generated by rope tension to be distributed and supported by both the one-way clutch and the hose clamp. While hose clamps are primarily designed as fasteners to secure hoses to fittings, in this application we are utilizing them to join two shafts by generating friction between the hose clamp and the shafts.

For the prototype shown in Fig 4, we used a shaft with a diameter of 22 mm and a hose clamp (Hi-Grip 304 Stainless 0XS, JCS) with a height of 13 mm and a weight of 22.48 g. This new design achieves a significant reduction in volume while maintaining a rotational radius nearly equivalent to that of conventional mechanism with two shaft collars.

As another alternative, we considered a method where the mating parts of two shafts are machined into a toothed shape, as shown in Fig. 5. After tensioning the rope, these teeth would be engaged. We explored various tooth shapes, including sawtooth, triangular, and rectangular waves. However, we found that machining teeth on the blank shaft would incur significant costs. Therefore, we selected hose clamps as an economical component capable of fixing the two shafts together. Another potential method involves using rigid couplings that can independently tighten two shafts. However, for a shaft diameter of 22 mm, the smallest coupling we could find (SRG-43C, SUNGIL) had dimensions of 43 mm outer diameter, 41 mm height, and a mass of 114 g per unit. In comparison, the mechanism proposed in this paper, which incorporates hose clamps, offers the potential for a lighter and more compact solution. For these reasons, we propose a tensioning mechanism utilizing hose clamps.

III. Allowable Torque Test of Hose Clamps

A. Experimental setup and method

To quantitatively evaluate the effectiveness of the proposed tensioning mechanism, we conducted a series of experiments to measure the maximum torque that could be sustained by a shaft fastened with a hose clamp before slippage occurred. The experimental apparatus is illustrated in Fig. 6. As shown in Fig. 6 (b), the two shafts, indicated by red and light blue colors, are connected via bearings, then secured axially with shaft collars and circumferentially with a hose clamp. These shafts were fabricated from SUS304 stainless steel. It should be noted that for these experiments, which aimed to measure the effect of hose clamp fastening, the one-way clutch was not inserted.

The hose clamps (Hi-Grip 304 Stainless 0XS, JCS) were designed for pipe diameters of 17-25 mm, selected to accommodate the 22 mm shaft diameter. This particular hose clamp has no slits, which are commonly found in hose clamps, thus potentially increasing frictional force with a large contact surface. To account for individual variations among hose clamps and to standardize conditions, preliminary tests were conducted. Shafts that had undergone sandblasting treatment with A80 were fastened with hose clamps, and the torque at which slipping occurred was measured. Hose clamps that yielded an average slipping torque within the range of 8.0-9.0 Nm over three trials were selected for use in the following experiments. It should be emphasized that these preliminary measurements were not included in the final experimental results.

As shown in Fig. 6 (c), the experimental apparatus was secured to an aluminum frame stand. The hose clamp was then tightened using a torque wrench (TRDC-030, eclatorQ) to a tightening torque of 7 Nm. To measure the maximum torque just before slippage occurred, a torque wrench was

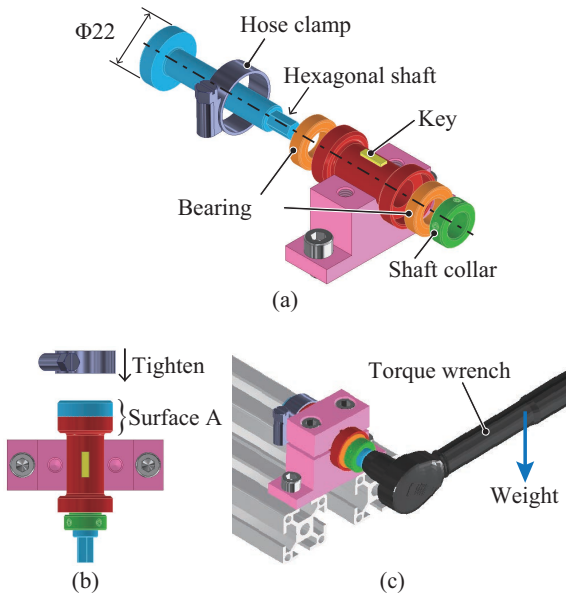

Fig. 6. Experimental setup. (a) Exploded view. (b) Top view. (c) Arrangement during experiment.

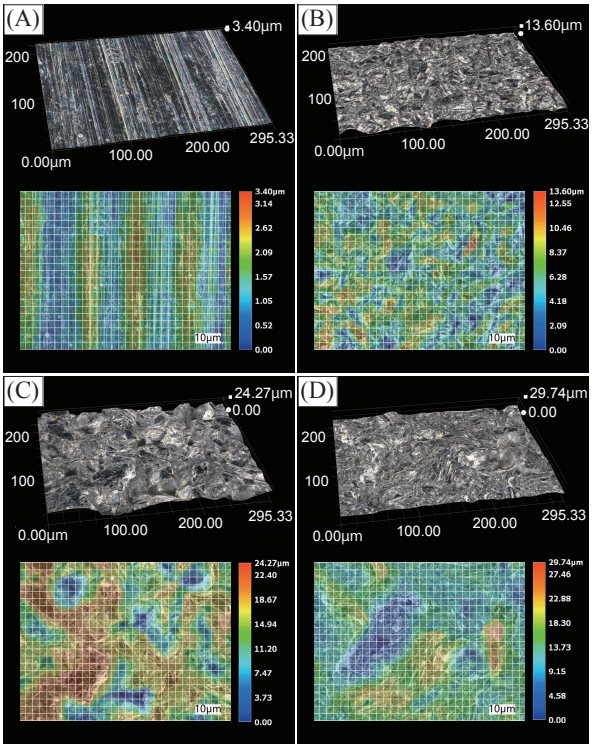

Fig. 7. Surface of the shafts. (A) A shaft with no additional processing. (B)-(D) Shafts blasted with A80, WA46, A24, respectively. All of these were observed at 1000x.

attached to the hexagonal head of the shaft. Weights of 1 kg each were then successively suspended from the torque wrench. The maximum torque was determined through visual observation. As the torque increased, the hose clamp and shaft would begin to slip gradually. For this experiment, the torque value at the moment when the torque wrench clearly moved was recorded as the measured value.

Three parameters were varied in the experiments: shaft, wire mesh, and hose clamp. First, four types of shafts were used, labeled (A), (B), (C), and (D), each differing in Surface A as shown in Fig. 6 (b). Shaft (A) was untreated, while shafts (B), (C), and (D) underwent sandblasting treatment on Surface A. This surface treatment was expected to increase the coefficient of friction between the shaft and the hose clamp by creating surface irregularities. For the blasting process, the following materials were used (all manufactured by Fuji Manufacturing):

- (B) Fuji Random A80 (particle size 150-212 μm)
- (C) Fuji Random WA46 (300-425 μm)
- (D) Fuji Random A24 (600-850 μm)

The surface conditions of each shaft are shown in Fig. 7. These images were captured using a digital microscope (VHX-8000, Keyence) at 1000x magnification. The upper row of images displays the three-dimensional surface topography of each shaft. The measured depths of the surface irregularities were as follows: 3.40 μm for shaft (A), 13.60 μm for shaft (B), 24.27 μm for shaft (C), and 29.74 μm for shaft (D). These are the difference between the maximum and minimum depths within the observation area. The lower row of images shows composite pictures of the same observed

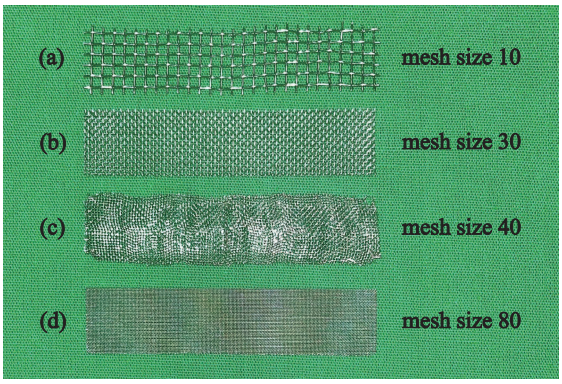

Fig. 8. Wire meshes used in the experiments. (a) mesh size 10, (b) 30, (c) 40, (d) 80. As the mesh size increases, the grid becomes finer and the wire diameter decreases.

areas, with the depth indicated by color coding. It should be noted that the scale varies for each condition, as indicated in the bottom right of each image. The grid lines are spaced at 10 μm intervals. These images clearly demonstrate that larger sandblasting particle sizes result in deeper and larger surface roughness.

Second, regarding the fastening method, several conditions were tested: one using only the hose clamp, and others where wire mesh shown in Fig. 8 was inserted between the shaft and the hose clamp. Wire meshes with four different levels of fineness (mesh sizes 10, 30, 40, and 80) were used. It should be noted that finer meshes are composed of thinner wire diameters. The experiments were conducted 12 times for each condition. For the untreated shaft fastened with only the hose clamp, 21 trials were performed. However, other exception to this procedure occurred during the course of the experiments. For the shaft (C) treated with WA46 blast, during testing with mesh size 80, the hexagonal head of the shaft became damaged, preventing further torque wrench measurements. Consequently, only 8 trials were completed for this condition and experiments with mesh sizes 10 and 30, as well as with blasted hose clamps, were not conducted for this shaft.

Finally, two types of hose clamps were utilized in the experiments: untreated clamps and clamps with their inner surfaces blasted using A24 abrasive. The experiments with blasted hose clamps were performed only with blasted shafts. This is because the combination of a blasted shaft and a blasted hose clamp was expected to increase the allowable torque. Tests were also conducted by replacing the hose clamp with a blasted one only under conditions where the highest allowable torque was obtained with wire meshes. It should be noted that these additional experiments were performed exclusively on shafts (B) and (D). For shaft (B), mesh size 80 was used, while for shaft (D), mesh size 30 was employed. These specific mesh sizes were selected based on their performance in previous trials with untreated hose clamps.

B. Results

The results of the experiment are presented in Fig. 9 and Table. I. The findings indicate that for shafts (B)-

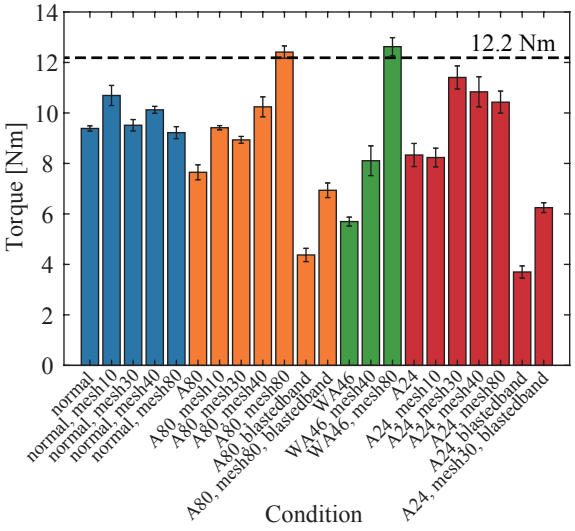

Fig. 9. Measured value in the experiments. Bars indicate average values with standard errors. From left to right, blue indicates the results for shaft (A) without any processing, orange for shaft (B) blasted with A80, green for (C) with WA46, and red for (D) with A24. The black dotted line shows the allowable torque of the one-way clutch, 12.2 Nm.

TABLE I

AVERAGE VALUE OF ALLOWABLE TORQUE MEASURED.

Conditions			Torque
Shaft	Hose clamp	Wire mesh	[Nm]
(A) Normal	normal	-	9.39 ± 0.10
	normal	10	10.69 ± 0.40
	normal	30	9.51 ± 0.23
	normal	40	10.12 ± 0.14
	normal	80	9.22 ± 0.24
(B) A80	normal	-	7.65 ± 0.30
	normal	10	9.42 ± 0.08
	normal	30	8.93 ± 0.14
	normal	40	10.24 ± 0.40
	normal	80	12.41 ± 0.25
	blasted	-	4.37 ± 0.26
	blasted	80	6.94 ± 0.29
(C) WA46	normal	-	5.70 ± 0.18
	normal	40	8.11 ± 0.59
	normal	80	12.63 ± 0.36
(D) A24	normal	-	8.33 ± 0.46
	normal	10	8.23 ± 0.37
	normal	30	11.41 ± 0.46
	normal	40	10.84 ± 0.60
	normal	80	10.43 ± 0.44
	blasted	-	3.70 ± 0.24
	blasted	30	6.25 ± 0.19

(D), which underwent sandblasting treatment, the allowable torque decreased when only the hose clamp was tightened, compared to the untreated shaft (A). However, when wire mesh was inserted between the shaft and the hose clamp, all shafts (A)-(D) exhibited an increase in allowable torque compared to the cases without wire mesh. Notably, some of the sandblasted shafts (B)-(D) with wire mesh achieved allowable torques exceeding 10.12 Nm, which was the value obtained for the untreated shaft (A) with wire mesh. These results suggest that while sandblasting treatment alone on the shaft's clamping area (Surface A) is insufficient, the combination of sandblasting and wire mesh can effectively enhance the allowable torque.

Regarding the types of wire mesh, the highest allowable torque was achieved with mesh size 80 for both the A80 blasted shaft (B) and the WA46 blasted shaft (C). The allowable torques were 12.41 Nm and 12.63 Nm respectively, surpassing the allowable torque of 12.2 Nm for the one-way clutch shown with black dotted line in the Fig. 9. For the A24 blasted shaft (D), the highest allowable torque was observed with mesh size 30. Under this condition, the allowable torque reached 11.41 Nm, which is lower than the allowable torque of the one-way clutch. However, this value still represents an improvement in allowable torque compared to the untreated shaft (A) with wire mesh and hose clamp, indicating a significant effect of the blasting treatment.

In experiments using sandblasted hose clamps, when these clamps were tightened without wire mesh, the measured allowable torque decreased significantly for both shafts (B) and (D). This reduction can be attributed to the decreased contact area resulting from the dents created on both the shaft and hose clamp surfaces due to the sandblasting process. When wire mesh was inserted between the sandblasted hose clamp and the shaft, the allowable torque increased compared to the case without wire mesh. However, this value was still lower than when using an untreated hose clamp with the same wire mesh. Specifically, the allowable torque decreased by 44% for shaft (B) and 45% for shaft (D) when compared to the untreated hose clamp with wire mesh.

To summarize, the experimental results reveal that the combination of sandblasting treatment on the shaft and the use of appropriate wire mesh significantly enhances the allowable torque of the tensioning mechanism. Optimal configurations surpassed the one-way clutch's limit, highlighting the importance of surface treatment and mesh selection in maximizing performance.

C. Discussion

First, we examine the combinations of wire mesh that resulted in the highest allowable torque for each shaft. As shown in Fig. 7, larger sandblasting particle sizes correspond to larger indentations on the shaft surface. Additionally, the wire diameter of the mesh increases as the mesh becomes coarser, with mesh size 80 at 110 µm, mesh size 40 at 165 µm, mesh size 30 at 215 µm, and mesh size 10 at 450 µm. The maximum average allowable torque was obtained with mesh 80 for shafts (B) and (C), and with mesh 30 for shaft (D). This suggests a potential correlation between the size of the indentations and the wire diameter of the mesh. These results indicate that the interlocking of the shaft surface irregularities with the wire mesh may increase the real contact area, thereby enhancing the friction coefficient.

Based on these results, we hypothesize that wrapping an appropriately coarse wire mesh around a sandblasted shaft and then tightening a hose clamp with sandblasted inner surface could further increase the allowable torque. Although our current tests showed a decrease in allowable torque with sandblasted hose clamps compared to untreated ones, we believe that by optimizing parameters such as the sandblasting particle size, blasting intensity, mesh size, and

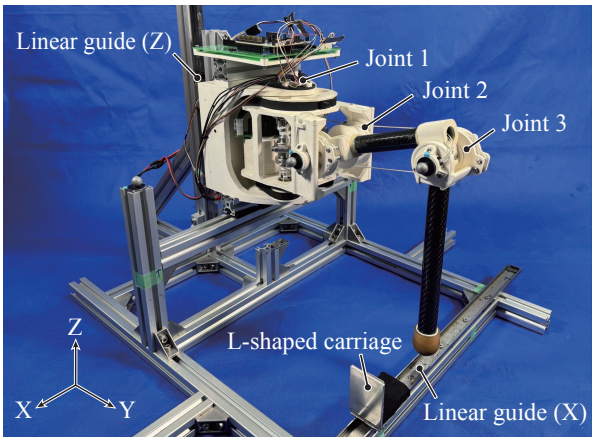

Fig. 10. TITAN-E1 monopod testing machine.

TABLE II
PARAMETERS OF WALKING.

Stride length	250 mm
Stride height	100 mm
Velocity in stance phase	200 mm/s
Duty ratio	0.5
Walking cycle	2.6 s

wire diameter, it may be possible to enhance the allowable torque.

IV. Application to a Leg Mechanism

To assess the practical applicability of the proposed tensioning mechanism in dynamic walking scenarios, we conducted a comprehensive simulated walking experiment by integrating a prototype tensioner into the TITAN-E1 monopod testing machine. For this experiment, we utilized a simplified version with only the hose clamp, without blast processing or wire mesh insertion. As explained in Chapter 2, TITAN-E1 is a quadruped robot with the leg mechanism shown in Fig. 2. Fig. 10 illustrates the overview of the monopod testing machine mounted on aluminum frames. The leg is fixed to a linear guide at the rear, allowing movement along the Z-axis. An L-shaped sheet is attached below the foot, movable along the X-axis on a linear guide, enabling simulated walking motions by placing the foot on this sheet. The machine weighs 3.5 kg, including electrical components. The experiment was conducted with an additional 6 kg payload. Table. II presents the walking parameters used in the experiment.

The results demonstrated that the one-way clutch did not sustain damage, and the machine operated continuously for 10,000 steps (7 hours and 13 minutes). Although this implementation only utilized the hose clamp, the experiment empirically confirmed the effectiveness of the proposed tensioning mechanism.

V. Conclusion

In this study, we have proposed a novel tensioning mechanism that combines a one-way clutch and hose clamps to increase its allowable torque. Through experiments with various conditions to enhance the friction force between the hose clamp and shafts, it was found that wrapping wire mesh around a sandblasted shaft before tightening the hose clamp significantly improved the allowable torque. Some configurations achieved allowable torque that exceeded the one of the one-way clutch. Additionally, a prototype of the proposed tensioner enabled prolonged walking trials without damage to the one-way clutch. These results experimentally demonstrate the applicability of the proposed tensioning mechanism for walking robots.

Ideally, the actual allowable torque of the proposed tensioner would be expected to be the linear sum of the allowable torques of the one-way clutch and the hose clamp. Experimental verification of this remains a topic for future work. Another approach involves using a shaft with equidistant semicircular grooves, paired pins, and a tightened hose clamp. Such refinements could potentially realize a tensioning mechanism capable of withstanding even higher torques than those achieved in this study, further enhancing its applicability to walking robots.

Acknowledgment

In preparing this paper, we received materials, information, and valuable advice from Otsuka Chemical Co., Ltd., as well as cooperation and guidance regarding 3D printing from Gutenberg Co., Ltd. We would like to express our deepest gratitude for their assistance. We also extend our sincere thanks to Ms. Kana Komiyama (Institute of Science Tokyo), Prof. Hiroki Akasaka (Institute of Science Tokyo), Prof. Naoyuki Takesue (Tokyo Metropolitan University), Prof. Yusuke Ota (Chiba Institute of Technology), and Prof. Takeshi Takaki (Hiroshima University) for their insightful comments and discussions.

References

[1] A. Mazumdar, S. J. Spencer, C. Hobart, J. Dabling, T. Blada, K. Dullea, M. Kuehl, and S. P. Buerger, "Synthetic fiber capstan drives for highly efficient, torque controlled, robotic applications," *IEEE Robotics and Automation Letters*, vol. 2, no. 2, pp. 554–561, 2017.

[2] H. In, H. Lee, U. Jeong, B. B. Kang, and K.-J. Cho, "Feasibility study of a slack enabling actuator for actuating tendon-driven soft wearable robot without pretension," in *2015 IEEE International Conference on Robotics and Automation (ICRA)*, 2015, pp. 1229–1234.

[3] S. Naruta and M. Uemura, "A Lightweight and Compact Tensioner for Wire-Driven Robots," in *The 39th Annual Conference of the Robotics Society of Japan*, no. AC2B2-06, 2021 (in Japanese).

[4] K. Tanaka and M. Hamaya, "Twist Snake: Plastic table-top cable-driven robotic arm with all motors located at the base link," in *2023 IEEE International Conference on Robotics and Automation (ICRA)*, 2023, pp. 7345–7351.

[5] L. Gerez and M. Liarokapis, "A Compact Ratchet Clutch Mechanism for Fine Tendon Termination and Adjustment," in *2018 IEEE/ASME International Conference on Advanced Intelligent Mechatronics (AIM)*, 2018, pp. 1390–1395.

[6] S. Kitano, S. Hirose, G. Endo, and E. F. Fukushima, "Development of lightweight sprawling-type quadruped robot TITAN-XIII and its dynamic walking," in *2013 IEEE/RSJ International Conference on Intelligent Robots and Systems*, 2013, pp. 6025–6030.

[7] S. Kitano, S. Hirose, A. Horigome, and G. Endo, "TITAN-XIII: sprawling-type quadruped robot with ability of fast and energy-efficient walking," *Robomech Journal*, vol. 3, pp. 1–16, 2016.

[8] S. Tsunoda, H. Nabae, K. Suzumori, and G. Endo, "Development of Quadruped Robot TITAN-E1 Using Plastic Structural Parts Printed by Fused Deposition Modeling," in *2022 JSME Conference on Robotics and Mechatoronics*, no. 2A1-Q07, 2022 (in Japanese).